Article

Relationships between the Curing Conditions and Some Mechanical Properties of Hybrid Thermosetting Materials

Newton L. Dias Filho,[*,a] *Celso X. Cardoso*[b] *and Hermes A. de Aquino*[a]

[a]*Departamento de Física e Química, Universidade Estadual Paulista, Av. Brasil, 56, Centro, CP 31, 15385-000 Ilha Solteira- SP, Brazil*

[b]*Departamento de Física, Química e Biologia, Universidade Estadual Paulista, Rua Roberto Simonsen, 305, 19060-900 Presidente Prudente-SP, Brazil*

Foi investigada a relação entre os parâmetros calor de polimerização (ΔH) e energia de ativação (E_a) obtidos por calorimetria diferencial de varredura (DSC) e a proporção entre resina epóxi e endurecedor de polímeros termorrígidos baseados em uma resina epóxi híbrida orgânica-inorgânica (OG). A energia de ativação (E_a) e o calor de polimerização (ΔH) aumentaram com o aumento do conteúdo de OG até 70% em massa. Um aumento adicional no conteúdo de OG até 80% reduziu E_a e ΔH. A análise dinâmico-mecânica sugere que a máxima densidade de ligações cruzadas é obtida em 83% de OG, enquanto as propriedades mecânicas de resistência à fratura e módulo de tensão são maximizadas em tôrno de 70% de OG.

The relationship between the heat of polymerization (ΔH) and activation energy (E_a) parameters, obtained by differential scanning calorimetry (DSC) and the ratio of epoxy resin to hardener of the thermosetting materials based on an organic-inorganic hybrid epoxy resin (OG) was investigated. Activation energy (E_a) and heat of polymerization (ΔH) increased with an increasing OG content, up to 70 wt%. Further increase in OG content to 80wt% reduced E_a and ΔH. Dynamic mechanical analysis indicates that the maximum cross-link density is obtained at 83 wt% OG, whereas fracture toughness and tensile modulus mechanical properties are maximized at 70 wt% OG.

Keywords: differential scanning calorimetry, siloxane, epoxy resin, silsesquioxanes, nanocomposites

Introduction

Epoxy resins are one of the most important classes of thermosetting polymers used for structural and adhesive applications.[1-5] However, the current problems in engineering applications of epoxy thermosets include poor resistance to crack propagation because they are brittle.[6,7] To overcome brittleness, among other additives of the multi-component formulation of the epoxy resin, a toughening agent is often used, such as fillers, polyhedral oligosilsesquioxanes, dendrimers etc.[8-18]

Methods of appropriately mixing two or more different materials, such as inorganic and organic, to obtain a new hybrid material with desirable features have been developed.[19-23]

Polymerization of the hybrid epoxy resin studied in this work, which is a nanosized epoxy resin, can lead to nanocomposite materials. In these materials the cubes of the cubic siloxane can be connected one another by organic components with known architecture and lengths of the order of 3-5 nm, forming composites with a completely defined interfacial component between the organic and inorganic phase.[19-23] This hybrid epoxy resin can be classified as a polyhedral oligomeric silsesquioxane, where the cubic silica cores are "hard particles" rigid with 0.53 nm diameter and a spherical radius of 1-3 nm including the peripheral organic units.[14-18]

It is known that different types of epoxy resins and curing conditions confer different characteristic properties. The purpose of this work is to apply a DSC technique to study the relationships between the curing conditions and some mechanical properties of the hybrid thermosetting materials.

*e-mail: nldias@dfq.feis.unesp.br

Experimental

Materials

Tetraethoxysilane [Si(OEt)$_4$], tetramethylammonium hydroxide [(CH$_3$)$_4$NOH], dimethylchlorosilane [HSi(CH$_3$)$_2$Cl], allyl glycidyl ether, and platinum dicyclopentadieno [Pt(dcp)], triphenylphosphine and methylenedianiline were purchased from Aldrich Chemical Company and used as received. Hexane and methanol was purchased from Lancaster Synthesis Company and used without further purification.

Synthesis of octaanion solution, [Me$_4$N$^+$]$_8$ [SiO$_{2.5}^-$]$_8$

[Me$_4$N$^+$]$_8$ [SiO$_{2.5}^-$]$_8$ was synthesized following a procedure previously reported, as described below.[19,24-27] A schematic representation of this reaction is shown in Figure 1. To a 2L round bottom flask equipped with a magnetic stir bar, were added 800.8 mL (7.60 mol) tetramethyl-ammonium hydroxide (25 wt% in methanol), 390.8 mL (9.92 mol) methanol, and 292.8 mL (16.26 mol) distilled water. The flask was cooled in an ice bath, and the system was maintained under nitrogen. Then 428 mL (1.91 mol) tetraethoxysilane was added *via* an addition funnel. The solution turned cloudy and was allowed to stir at room temperature overnight to produce a clear solution of tetramethylammonium octaanion in quantitative yield.

This solution was characterized by ^{29}Si NMR, that showed one peak at δ -99.4 ppm.

Synthesis of octa[hydridodimethylsiloxy]octasiloxane, [HMe$_2$SiOSiO$_{1.5}$]

[HMe$_2$SiOSiO$_{1.5}$] was also synthesized following published procedures, as it is described below.[19,24-27] Figure 1 shows a schematic representation for this reaction.

To a 5 L bottom flask equipped with a mechanical stirrer, were added 2600 mL hexane and 436 mL (4.0 mol) dimethylchlorosilane under nitrogen. The flask was placed in an ice bath and 1000 mL of the octaanion solution was then added *via* an addition funnel, over a 2h period. The final mixture was stirred continuously for another 2h. The two layers were separated with a separatory funnel. The hexane layer was dried over sodium sulfate and gravity filtered, followed by solvent removal by rotary evaporation to yield a white powder. This powder was rinsed with methanol and collected by vacuum filtration. The product was dried in a vacuum oven at 70 °C for 5 h, obtaining a white powder in 89 g yield, which was 70% of theoretical.

^{1}H NMR showed a multiplet at δ 4.73 (m, 8H, CH$_3$-Si-<u>H</u>) and doublet at 0.26, 0.25 ppm (d, 48H, C<u>H</u>$_3$-Si-H) ppm. ^{13}C NMR revealed one peak at δ 0.059 ppm (H-Si-<u>C</u>H$_3$). ^{29}Si NMR showed two peaks at δ – 2.897 ppm (H-<u>Si</u>-CH$_3$) and -108.697 ppm (<u>Si</u>-O$_4$). SEC: Mn = 995, Mw = 1008, PDI = 1.01, calculated MW = 1017 g mol^{-1}. FTIR (KBr) ν_{max}/cm^{-1}: 2966 (ν C-H), 2144 (ν Si-H), 1420 (ν C-H), 1258 (ν Si-CH$_3$), 1096 (ν Si-O).

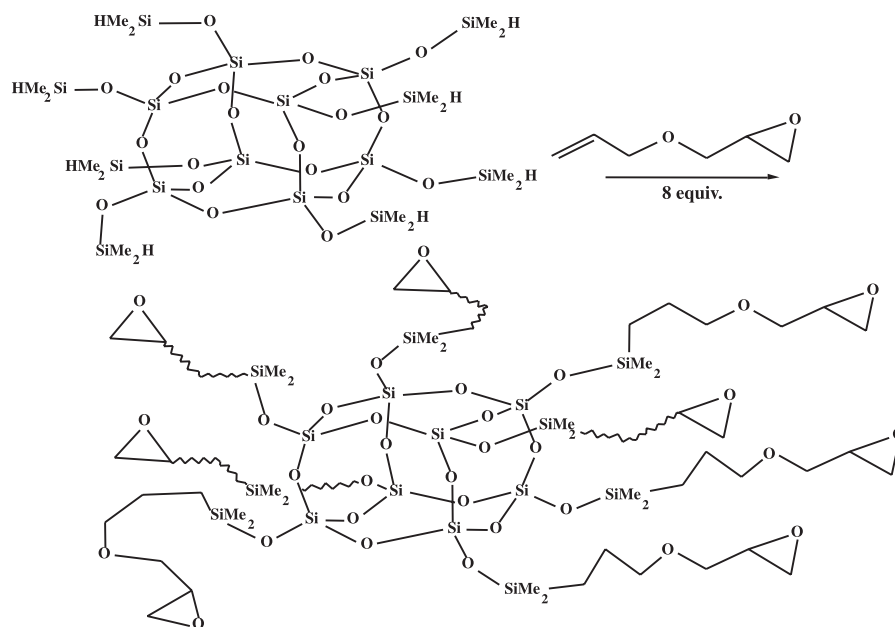### *Synthesis of octa[dimethylsiloxypropylglycidylether] octasiloxane (OG)*

The synthesis of OG followed published procedures, as described below.[19,27] A schematic representation for this reaction is showed in the Figure 2.

To a 500 mL schlenk flask equipped with a magnetic stir bar and a condenser, was added 120.0 g (0.12 mol) octahydrido spacer cube, [HMe$_2$SiOSiO$_{1.5}$]. The flask was evacuated and refilled with N$_2$ gas three times at 50 °C. Then 132.0 mL (0.99 mol) allyl glycidyl ether was added to the solution followed by 0.3 mL of 2.0 mmol L^{-1} solution of platinum dicyclopentadieno [Pt(dcp)] and the reaction was heated at 90 °C. Triphenylphosphine, 10 mg, was then added to deactivate the [Pt(dcp)] catalyst and the toluene solvent was removed by rotary-evaporation. Yield: 210 g (91% of theoretical).

This material was characterized as follows. ^{1}H NMR (CDCl$_3$) δ C<u>H</u>$_2$O(CH$_2$)$_3$ diastereotopic 3.55, 3.30 (dd, *J* 3.27 Hz, 8H) (due to peak overlap, all resonances between 3.34 and 3.16 are integrated as two peaks, 24H), 3.30, 3.28 (dd, *J* 2.89 Hz), SiCH$_2$CH$_2$C<u>H</u>$_2$O 3.18 (m, 8H), OC<u>H</u>$_2$CH (epoxy) 2.94 (m, 8H), C<u>H</u>$_2$ (epoxy) diastereotopic 2.58 (dd, 8H),
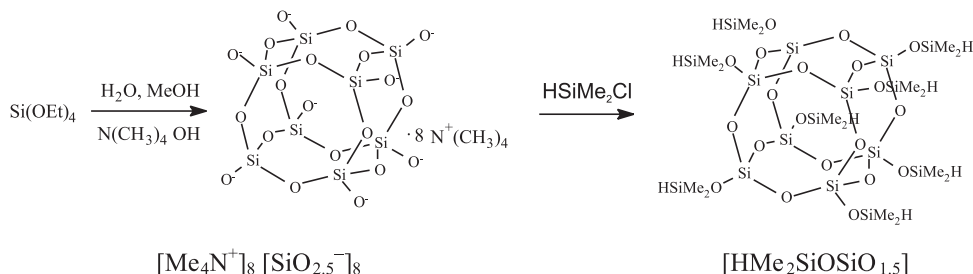
Figure 1. Schematic representation of preparation of the octaanion solution, [Me$_4$N$^+$]$_8$ [SiO$_{2.5}^-$]$_8$, and of the octa[hydridodimethylsiloxy] octasiloxane, [HMe$_2$SiOSiO$_{1.5}$].

Figure 2. Reaction of preparation of the octa[dimethylsiloxypropylglycidylether] octasiloxane (OG).

2.40 (dd, 8H), SiCH$_2$C$\underline{H}_2$CH$_2$O 1.48 (m,16H), SiC$\underline{H}_2$CH$_2$CH$_2$O 0.47 (m, 16H), (C$\underline{H}_3$)$_2$SiCH$_2$ 0.00 ppm (s, 48H). ^{13}C NMR (CHCl$_3$) δ SiCH$_2$CH$_2$$\underline{C}H_2$O 74.29, $\underline{C}$H$_2$O(CH$_2$)$_3$ 71.86 , OCH$_2$$\underline{C}$H (epoxy) 51.11, $\underline{C}$H$_2$ (epoxy) 44.35, SiCH$_2$$\underline{C}H_2CH_2$O 23.59, Si$\underline{C}H_2CH_2CH_2$O 13.93, ($\underline{C}H_3$)$_2$SiCH$_2$ 0.00 ppm. ^{29}Si NMR (C$_6$D$_6$) δ (CH$_3$)$_2$$\underline{Si}CH_2$ -7.3, $\underline{Si}$OSi(CH$_3$)$_2$CH$_2$ -129.4 ppm. SEC: Mn = 1850, Mw = 1898, PDI = 1.02 , calculated MW = 1931 g mol^{-1}.

FT-IR (neat film) ν_{max}/ cm^{-1}: (C-H) 3035, 2962, 2934, 2874 (m); (Si-H) 2142 (m); (Si-CH$_3$ and C-O) 1250-1260 (s); (Si-O) 1095 (vs); (C-O-C) 902 (s).

Curing process

The hybrid epoxy resin (OG) is a viscous liquid and the curing agent 3,3-methylenedianiline (MDA) is solid at room temperature. The structures of the OG and MDA are shown in Figure 3.

In the present investigation, samples having different amount of OG and MDA were prepared. In formulating samples, the molar ratio f is defined as the ratio of epoxy ring to amine hydrogen (ϕ = no. of epoxy rings in OG/ No. of amine hydrogen in MDA).

A conventional stoichiometric ratio of 1 mol of epoxy resin in OG (1 mol of OG contain 8 mol of epoxy rings) to 2 mol of amine (2 mol of MDA contain 8 amine hydrogen) would occur for ϕ = 1. Thus, when ϕ = 1, the two components are mixed at stoichiometric amount of 83 wt% of OG and 17 wt% of MDA.

For curing optimization tests, samples were cured at different temperatures and times to study the cure condition.
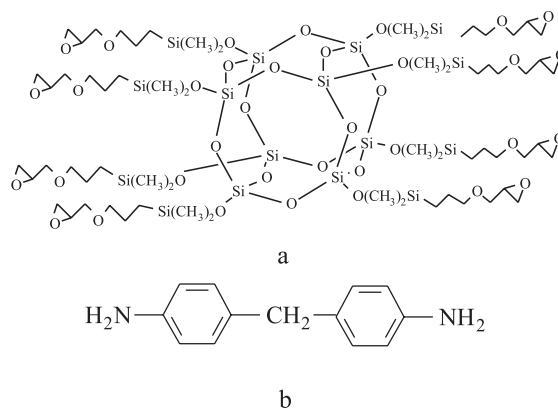
Figure 3. Components of the curing reaction: (a) OG; (b) 3,3-methylenedianiline (MDA).

OG/MDA samples were cured in the temperature range of 100- 200 °C and for periods of 2 to 12 h. In the present study curing for 10h at 150 °C was adopted for the composites OG/MDA.

OG and MDA were weighed into an aluminum pan with a diameter of 61.5 mm and depth of 18 mm and mixed by hand at room temperature. The mixture was then put into an oven preheated to ~150 °C under vaccum. After degassing for 10-15 min and no more bubbles emerged from the mixture, the content was transferred to an aluminum mold preheated to 150 °C. It is not observed any reaction during vacuum degassing at 150 ºC. The filled mold was placed in an oven and heated under nitrogen for 10 h at 150 °C for curing the mixture. After the mold cooled, the sample was removed and kept in a sealed desiccator before the dielectric analysis and mechanical tests were performed.

The compositions of samples are shown in Table 1. A schematic representation of composites with discontinuous organic-inorganic phases from cubic silsesquioxane is shown in Figure 4.

Table 1. Formulations for OG/MDA composites

wt% OG	wt% MDA	φ*	Molar ratio MDA/OG
95	5	3.90	0.51
91	9	2.07	0.96
87	13	1.37	1.46
83	17	1.00	1.99
80	20	0.82	2.44
79	21	0.77	2.59
77	23	0.69	2.91
73	27	0.55	3.60
70	30	0.48	4.18
68	32	0.44	4.58
67	33	0.42	4.79
63	37	0.35	5.72
60	40	0.31	6.49
55	45	0.25	7.96
50	50	0.20	9.74
40	60	0.14	14.62
30	70	0.09	22.78
20	80	0.05	38.80

*In formulating samples, the molar ratio f is defined as the ratio of epoxy ring to amine hydrogen (φ = number of epoxy rings in OG/number of amine hydrogen in MDA).

Mechanical testing

Samples removed from the aluminum mold had rough edges due to the overflow of polymer. These edges were polished using a polish wheel with 120-grit SiC paper. After polishing, the samples were ready for mechanical testing. The average dimensions of the samples were $3.0 \times 13.0 \times 170$ mm. (errors $< \pm 0.2$ for width and thickness and $< \pm 0.4$ for length).

The elastic moduli (tensile moduli), E, data were obtained using an Instron 4502 screw driven mechanical testing machine. The dimensions of each sample were determined by measuring the width and thickness at three points along the gauge length prior to the test. These were used to calculate the averages of width and thickness for each sample. The elastic moduli were obtained following ASTM standard [No. E111(1997)]. The samples were clamped using anti-slackening screw grips with added friction increasing pads. Care was taken to ensure that the tensile and sample axes were co-axial. The cross-head displacement rate was set at 1 mm min^{-1}. The tensile tests were stopped when the samples were in the elastic deformation region. Usually, tests were stopped at loads of about 200 – 250N. Samples with very low modulus would break before reaching this load. The data acquisition software collected load-displacement data points at a speed of 2 points *per* second.

The critical stress intensity factor (fracture toughness) was obtained following ASTM standard [No. E399(1990)]. This standard requires that the ratio of width to thickness be between two and four, and the ratio of the pre-crack to sample between 0.45 and 0.55. The pre-crack was introduced using a fresh razor blade tapped into a square notch sawed to 0.1 - 0.2 of the sample width. This method introduces a natural crack into the sample. Then the sample was loaded into the testing apparatus in the same manner as described above for Young's modulus measurements. The sample was then loaded to failure and the breaking load recorded. The critical stress intensity factor was determined from the standard relationships:
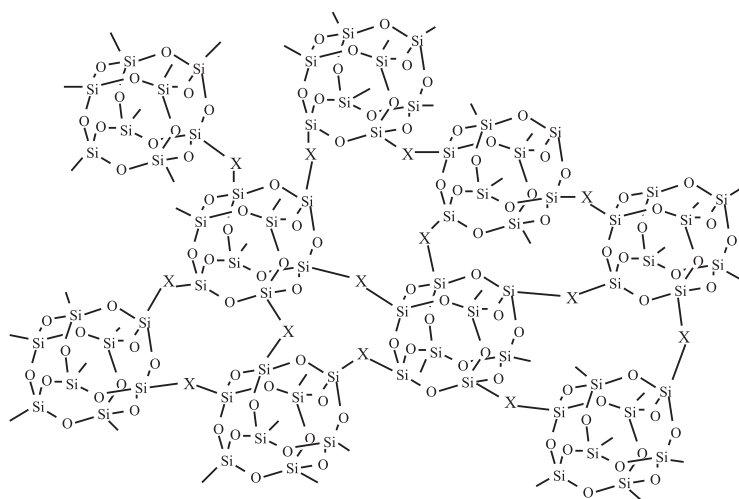
Figure 4. Scheme of a general representation of composites with discontinuous organic-organic phases from cubic silsesquioxane. X = links between cubes.

$$K_{IC} = Y\sigma_0 a^{1/2}$$

$$Y = \left[1.99 - 0.41(\frac{a}{w}) + 18.70(\frac{a}{w})^2 - 38.48(\frac{a}{w})^3 + 53.85(\frac{a}{w})^4\right]$$

$$\sigma_0 = \frac{P_b}{Bw}$$

where P_b is the load at break, B is the sample thickness, w is the sample width, and a is the pre-crack length.

NMR and FTIR Analyses

Solution NMR Analyses. All ^1H and ^{13}C NMR analyses were done in $CDCl_3$ and recorded on a BRUKER DRX 400 spectrometer. ^{13}C NMR spectra were obtained at 100.6 MHz using a 27027 Hz spectral width, and a relaxation delay of 0.6 s. ^1H NMR spectra were collected at 400.1 MHz, using a 3591 Hz spectral width, and a relaxation delay of 1 s.

Solid state NMR analyses. All ^{29}Si-NMR (59.5 MHz) and ^{13}C NMR (75.4 MHz) solid state analyses were recorded on a Varian INOVA 300 spectrometer. The samples were packed in zirconia rotors and spun at the magic angle at 4500 Hz, after a relaxation delay of 10.0 and 6.0 s for ^{29}Si and ^{13}C respectively. All chemical shifts are reported in units (ppm) using TMS as external reference.

Gel permeation chromatography (GPC). GPC data were measured using a Waters GPC system, equipped with RI and UV detectors, a Styragel column set, and a data capture unite. The system was calibrated using polystyrene standards, with THF used as the eluent.

Fourier transform infrared spectra was recorded on a Nicolet 5DXB FT-IR 300 spectrometer. About 600 mg of KBr were ground in a mortar and pestle, and a sufficient quantity of the solid sample was ground with KBr to produce a 1wt% mixture resulting in pellets. Liquid samples were cast on salt plates. A minimum of 32 scans was collected at a resolution of ± 4 cm^{-1}.

Differential Scanning Calorimetry (DSC)

Curing behavior of OG with MDA was monitored with a Perkin-Elmer DSC7 type differential scanning calorimeter, at temperatures ranging from 25 to 200 °C. The resin/hardener mixture (18-22 mg) was heated in aluminum pans at a heating rate of 10 °C min^{-1} in nitrogen atmosphere or in static air atmosphere. Pure indium was used as a standard for calorimetric calibration. Runs were carried out using an empty cell as a reference. The heat flow data, as a function of temperature and time, were obtained using the area under the peak of the exotherm.

Dynamic Mechanical Analysis (DMA)

DMA was performed on cured samples using a Netzsch DMA 242 instrument operating at 1 Hz in the three-point bending mode at a heating rate of 5 °C min^{-1}. The dimensions of the specimens were ~ 3.1 × 10 × 100 mm. Dynamic mechanical spectra were obtained from – 50 to 200 °C.

Results and Discussion

Curing parameters from DSC

Differential scanning calorimetry (DSC) has been extensively used to study the curing reaction kinetics of various thermosetting polymers.[28] DSC measures the heat flow of the sample as a function of temperature. The basic assumption for the application of DSC technique to the cure of the thermoset composites is that the rate of the kinetics process (dα/dt) is proportional to the measured heat flow (dH/dt),[29-31] or,

$$d\alpha/dt = dH/dt \tag{1}$$

where H is the enthalpy of the curing reaction.

Without knowing the exact reaction mechanism, it is reasonable to assume that the kinetics parameters of the curing process at a given time t is only a function of the conversion fraction α, or,

$$d\alpha/dt = K_{(T)}f(\alpha) \tag{2}$$

where $K_{(T)}$ is the temperature-dependent reaction rate constant, which is usually assumed to be of the Arrhenius form, and $f(\alpha)$ is a dependent kinetic model function.

Therefore, the rate constant $K_{(T)}$ is dependent on temperature and follows a relationship of Arrhenius type as in equation (3),

$$K_{(T)} = Z \exp[-E_a/RT] \tag{3}$$

where Z is the pre-exponential factor, R the universal gas constant (8.314 J $mol^{-1}K$), and T is the absolute temperature.

The kinetic parameters of the curing reaction, with special reference to such as E_a, can be calculated using various computational methods.[32] As it is well known, the reaction between epoxies and amines involves several steps,[33] and hence the kinetics may be rather complex. Without knowing the exact reaction mechanism, it is reasonable to assume that the kinetic parameters of the curing process can be described by the Borchardt and

Daniels method,[32] in which the reaction rate at a given time *t* is a function of the conversion fraction α, or

$$d\alpha/dt = K_{(T)} (1 - \alpha)^n \tag{4}$$

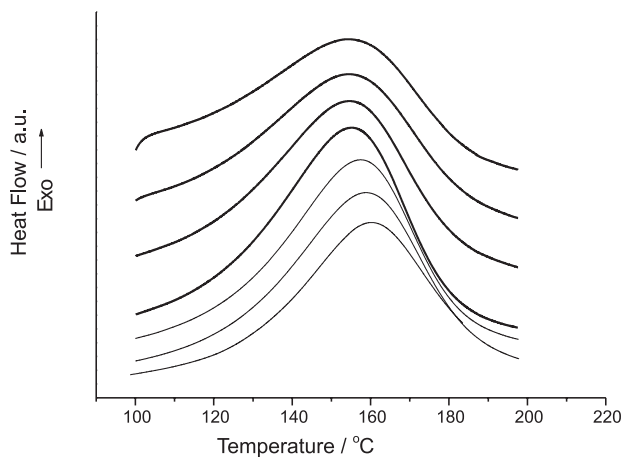where n is the reaction order kinetic, and $K_{(T)}$ is the temperature-dependent reaction rate constant.

The reaction rate ($d\alpha/dt$) was obtained by dividing the peak height at temperature T by the total peak area. The unreacted fraction ($1 - \alpha$) was obtained by measuring the ratio of the partial area at temperature T to the total peak area and subtracting it from unity. The reaction order *n* and $K_{(T)}$ were obtained from the plot of log $d\alpha/dt$ *versus* log$(1 - \alpha)$.

The Borchardt and Daniels method[32] assumes that the apparent activation energy, E_a, can be calculated using the Arrhenius expression,

$$\ln K_{(T)} = \ln (Z) - E_a/RT \tag{5}$$

From the slope of a linear-fit line, the activation energy, E_a can be calculated, *i.e.*, the slope of $\ln(K_{(T)})$ *versus* 1/T gives the value of E_a. The best fit was obtained using n $\cong$ 2, indicating that the curing reaction follows a second-order kinetcs.
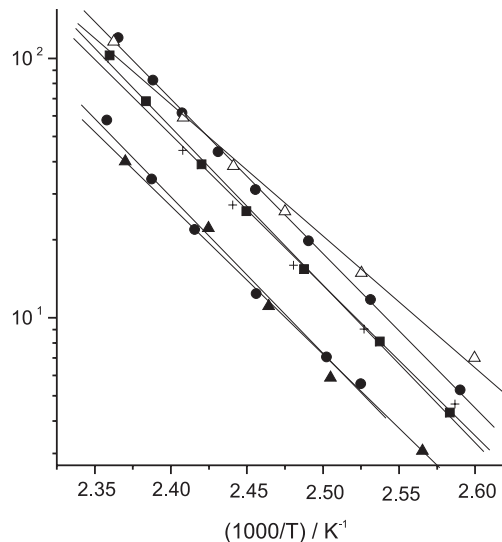
Figure 5 plots several DSC curves of the OG/MDA composites obtained at temperatures ranging from 100 to 200 °C.

Figure 6. Arrhenius plots for OG/MDA composites at several OG contents (wt%): Δ20, +30, $\blacklozenge$40, $\blacksquare$ 60, $\bullet$ 70. In this figure $K_{(T)}$ is plotted on a ln-scale against 1000/T. The slope of the linear fit is E_a/R.

Figure 7. Heat of polymerization (ΔH) for OG/MDA composites *versus* OG content.
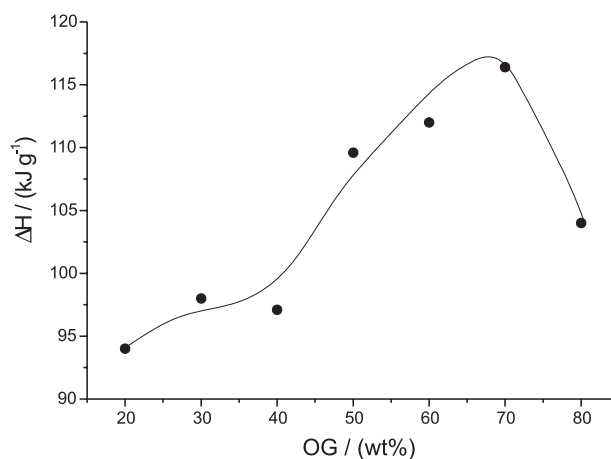

Figure 5. DSC curves for OG/MDA composites at several OG contents: 20, 30, 40, 50, 60, 70, 80 wt%, from bottom to top.

Arrhenius plots from DSC scans recorded for the cured samples using equation 2 are straight lines, the slope (E_a/R) of which gives the value of E_a, as shown in Figure 6.
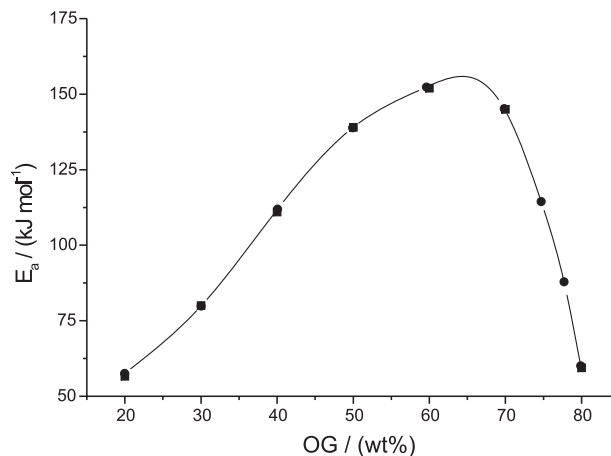
The curves of heat of polymerization (ΔH) and activation energy (E_a) *versus* OG content are shown in Figures 7 and 8, respectively. Both curves of ΔH and E_a show the same profile with respect to OG content. They
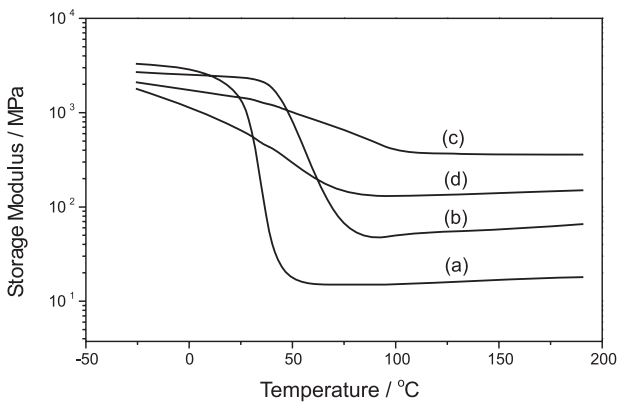

Figure 8. Activation energy (E_a) for OG/MDA composites *versus* OG content.

exhibit maxima in the region of ~70 wt% OG. E_a and ΔH increase with increasing wt% OG up to around 70 wt%. Further increase in concentration of OG up to 80 wt% reduce E_a and ΔH.
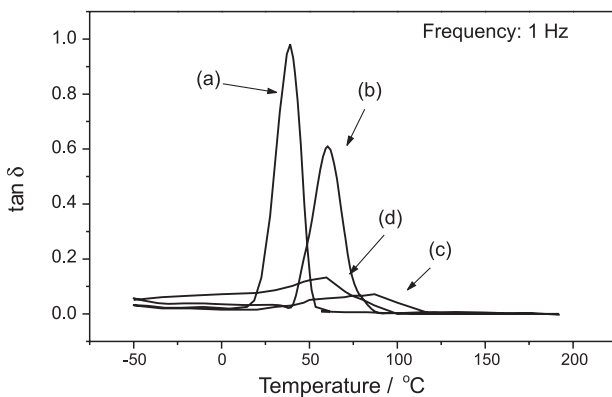
Relationships between curing parameters and dynamic mechanical analysis and mechanical properties

Figures 9 and 10 show the DMA of OG/DMA composites. In Figure 9 the maximum rubbery state modulus is found at $\phi = 1$. As the rubbery state modulus relates directly to the network cross-link density, the maximum cross-link density is expected at $\phi = 1$ (83 wt% OG and 17 wt% of MDA, corresponding to stoichiometric ratio), which appears in DMA as the maximum rubbery state modulus (Figure 9) and the highest T_g (Figure 10).

On the other hand, fracture toughness and tensile modulus mechanical properties show the same profile with respect to OG content, in the sense that they exhibit maxima at $\phi \approx 0.50$ (≈ 70 wt% OG and 30 wt% of MDA, corresponding to an "excess" of MDA), as is shown in Figures 11 and 12, respectively.

Thus, dynamic mechanical analysis indicates that the maximum cross-link density is obtained at 83 wt% OG, whereas fracture toughness and tensile modulus mechanical properties are maximized at 70 wt% OG.

It is known that for conventional epoxy resin, such as DGEBA, the highest cross-link densities are obtained at stoichiometries where two epoxy ring equivalents are mixed with one amine group equivalent (corresponding to stoichiometric point: the ratio of epoxy ring to amine hydrogen is 1:1, and $\phi = 1$). Most epoxy thermoset materials exhibit the maximum tensile modulus values for stoichiometries of $\phi = 1.0$ (ϕ is defined as the molar ratio of epoxy ring in conventional epoxy *per* amine hydrogen). Fracture toughness also increases as the amine content increases below $\phi = 1$.

For the OG/MDA composites the highest cross-link density which would be obtained at $\phi = 1$ (83 wt% OG) implies that the dominating structure is expected to be

Figure 9. Storage modulus for OG/MDA composites at various OG contents (wt%): (a) 63, (b) 73, (c) 83, (d) 91.

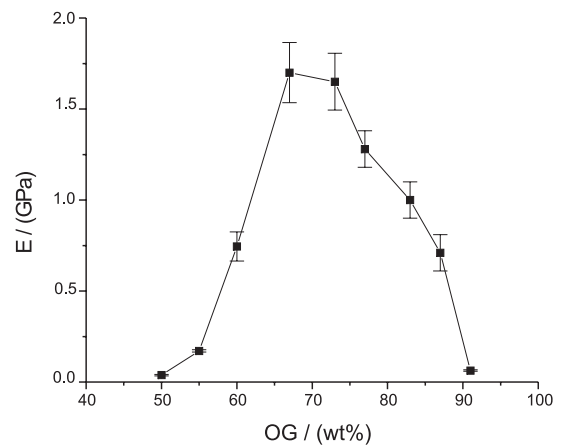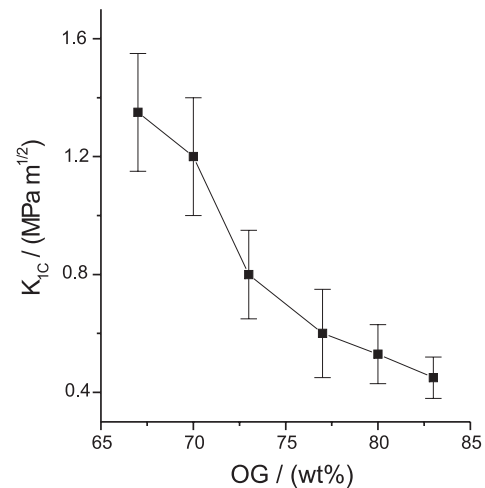**Figure 10.** tan δ for OG/MDA composites at various OG contents (wt%): (a) 63, (b) 73, (c) 83, (d) 91.

Figure 11. Tensile modulus (E) for OG/MDA composites *versus* OG content. Each data point represents an average of at least five samples.

Figure 12. Fracture toughness (K_{1C}) for OG/MDA composites *versus* OG content. Each data point represents an average of at least five samples.

the one in which MDA is tetrafunctional on curing, e.g. connecting four cubes.

On the contrary, for the OG/MDA composites, the maximum modulus and fracture toughness are obtained at $\phi \approx 0.50$ ($\approx$ 70 wt% OG), and maintains its maximum modulus up to $\phi \approx 0.40$, which are not compositions where the highest cross-linked density are reached. This implies that the best mechanical properties are provided by some degree of chain flexibility.

This can be tentatively explained based on the fact that before occurring the complete reaction and cross-link between all the amines and epoxy rings, it becomes very difficult for unreacted functional groups to find each other due to increasing of the viscosity during curing. These unreacted functional groups will remain as pendant groups. Then, for $\phi < 1.0$, the excess increasing of MDA causes increased motion of organic tethers (links between cubes) by increasing the number of pendants groups and/or decreasing cross-link density. The other possibility is that the steric hindrance should be greater for bulky OG than for conventional epoxy, such as DGEBA. In this case, the reaction of the first hydrogen of the NH_2 group should be favored over the second one, resulting in a uniform and densely cross-linked structure that can be obtained at $\phi \approx 0.50$. In this case, the dominating structure is expected to be the one in which MDA is bifunctional on curing (linear tethers connecting two cubes).This assumption (MDA is bifunctional connecting two cubes) seems to be favored taking into consideration that the highest values of ΔH (heat of polymerization, E_a (obtained from DSC), E (tensile modulus), and K_{1C} (fracture toughness), occur in a ratio of ~ 4 mol of MDA to 1 mol of OG corresponding to $\phi \approx 0.50$.

For instance, when DGEBA is cured with excess MDA the material changes from ductile to a brittle material, both tensile modulus and fracture toughness increase from $\phi = 1.0$ to $\phi = 0.5$, and, then, they drop significantly.[19] Therefore, while epoxy resin/hardener conventional systems become brittle with excess of curing agent ("Excess" MDA is used for $\phi < 1.0$), OG/MDA composites become rubbery. At $\phi \approx 0.14$, the modulus data of OG/MDA cannot be measured because of the rubberlike behavior. On the other hand, for composition at $\phi > 2.0$ ("Excess" OG) OG/MDA composites become viscous. Consequently, at $\phi > 2.0$, the modulus of OG/MDA cannot be measured, and no data points are included in Figure 9. This behavior also reflects in the fracture toughness, and no data points for $\phi < 0.45$ and $\phi > 2.0$ are included, because it is practically impossible to introduce a natural crack into these samples.

Conclusions

The cure kinetic of a hybrid epoxy resin, denominated octa[dimethylsiloxypropylglycidylether] octasiloxane (OG), in presence of 3,3-methylenedianiline (MDA) as hardener, was examined by DSC technique at various experimental conditions.

The results of heat of polymerization and activation energy obtained by DSC technique show the same profile with respect to OG content, in the sense that they exhibit maxima around 70 wt% OG ($\phi \approx 0.50$).

Dynamic mechanical analysis suggests that the maximum cross-link density is obtained at 83 wt% OG ($\phi = 1$, components are mixed at stoichiometric amount), whereas fracture toughness and tensile modulus mechanical properties are maximized at 70 wt% OG ($\phi \approx 0.50$). Thus, this formulation of $\phi \approx 0.50$ containing excess of amine, is not the composition where the highest cross-linked density is reached for the OG/MDA composites. This implies that the best mechanical properties and curing parameters are provided by some degree of chain flexibility.

These results indicated that these techniques can be used to study the curing conditions of hybrid epoxy resins based on cubic silsesquioxanes. Furthermore, the results these techniques can be used to know and to understand the relationships between the structure of the networks and the final properties.

Acknowledgments

References

1. Mark, H. F.; Bikales, M. N.; Overberger, C. G.; Mengues, G.; *Encyclopedia of Polymer Science and Engineering, Emulsion Polymerization to Fibers, Manufacture*, John Wiley & Sons: New York, 1986.

2. Lee, H.; Neville, K.; *Handbook of Epoxy Resins*, McGraw Hill: New York, 1967.

3. Mauri, A. N.; Riccardi, C. C.; Williams, R. J. J.; *Polym. Bull.* **2001**, *45*, 523.

4. Pellice, S. A.; Fasce, D. P.; Williams, R. J. J.; *J. Polym. Sci.* **2003**, *41*, 1451.

5. Smith, I. T.; *Polymer* **1961**, *2*, 95.

6. Yamini, S.; Young, R. J.; *J. Mat. Sci.* **1980**, *5*, 1814.

7. Yamini, S.; Young, R. J.; *J. Mat. Sci.* **1980**, *15*, 1823.

8. Zhang, C.; Laine, R. M.; *J. Organomet. Chem.* **1996**, *521*, 199.

9. Lee, A.; Lichtenhan, J.D.; *Macromolecules* **1998**, *31*, 4970.

10. Rey, L.; Poisson, N.; Maazouz, A.; Sautereau, H.; *J. Mat. Sci.* **1999**, *34*, 1775.

11. Li, Z. G.; Wang, L.; Toghiani, H.; Daulton, T. L.; Koyma, K.; Pittman Jr., C.U.; *Macromolecules* **2001**, *34*, 8686.

12. Abad, M. J.; Barral, L.; Fasce, D. P.; Williams, R. J. J.; *Macromolecules* **2003**, *36*, 3128.

13. Fu, B. X.; Namani, M.; Lee, A.; *Polymer* **2003**, *44*, 7739.

14. Ni, Y.; Zheng, S.; Nie, K.; *Polymer* **2004**, *45*, 5557.

15. Voronkov, M. G.; Lavrent'yev, V. I.; *Top. Curr. Chem.* **1982**, *102*, 199.

16. Baney, R. H.; Itoh, M.; Sakakibara, A.; Suzuki, T.; *Chem. Rev.* **1995**, *95*, 1409.

17. Provatas, A.; Matisons, J. G.; *Trends. Polym. Sci.* **1997**, *5*, 327.

18. Feher, F. J.; Budzichowski, T. A.; *J. Organomet. Chem.* **1989**, *379*, 33.

19. Laine, R. M.; Asuncion, M.; Baliat, S.; Dias Filho, N. L.; Harcup, J.; Sutorik, A. C.; Viculis, L.; Yee, A. F.; Zhang, C.; Zhu, Q. In *Organic/Inorganic Hybrid Materials*; Klein, L.; De Guire, M.; Lorraine, F.; Mark, J., eds.; MRS Symp. Ser. vol. 576, 1999, pp. 3-14; Dias Filho, N. L., unpublished work.

20. Laine, R. M.; Choi, J.; Lee, I.; *Adv. Mat.* **2001**, *13*, 800.

21. Choi, J.; Yee, A. F.; Laine, R. M.; *Macromolecules* **2003**, 36, 5666.

22. Choi, J.; Tamaki, R.; KIM, S. G.; Laine, R. M.; *Chem. Mat.* **2003**, *15*, 3365.

23. Choi, J.; Kim, S. G.; Laine, R. M.; *Macromolecules* **2004**, *37*, 99.

24. Hasegawa, I.; Kuroda, K.; Kato, C.; *Bull. Chem. Soc. Jap.* **1986**, *59*, 2279.

25. Hasegawa, I.; Sakka, S.; Sugahara, Y.; Kuroda, K.; Kato, C.; *J. Chem. Soc. Chem. Comm.* **1989**, 208.

26. Hasegawa, I.; Ishida, M.; Motojima, S.; *Synth. React. Inorg., Met.-Org., Nano-Met. Chem.* **1994**, *24*, 1099.

27. Sellinger, A.; Laine, R. M.; *Chem. Mater.* **1996**, *8*, 1592.

28. Prime, R.B. In *Thermal Characterization of Polymeric Materials*, 2nd ed., Academic Press: San Diego, 1997, vol. 2, ch. 6.

29. Varma, I. K.; Bhama, P. V. S.; *J. Comp. Mat.* **1986**, *20*, 411.

30. He, Y.; *Thermochim. Acta* **2001**, *367*, 101.

31. Rosu, D.; Cascaval, C. N.; Mustata, F.; Ciobanu, C.; *Thermochim. Acta*, **2002**, *383*, 119; Rosu, D.; Mustata, F.;Cascaval, C.N.; *Thermochim. Acta*, **2001**, *370*, 105.

32. Borchardt, H.J.; Daniels, F.; *J. Am. Chem. Soc.* **1956**, *79*, 41; Barret, K.E.J.; *J. Appl. Polym. Sci.* **1967**, *11*, 1617; Kissinger, H. E.; *Anal. Chem.* **1957**, *29*, 1702; Malek, J.; *Thermochim. Acta* **1992**, *200*, 257; Malek, J.; *Thermochim. Acta* **2000**, *355*, 239.

33. Urbaczewski, E.; Pascault, J. P.; Sautreau, H.; Riccardi, C. C.; Moschiar, S. S.; Williams, R. J. J.; *J. Makromol. Chem.* **1990**, *191*, 943; Mijovic, J.; Kim, J.; Slaby, J.; *J. Appl. Polym. Sci.* **1984**, *29*, 1449; Riccardi, C. C.; Williams, R. J. J.; *J. Appl. Polym. Sci.* **1986**, 32, 3445.